3rd US-European Competition and Workshop on Micro Air Vehicle Systems (MAV07) & European Micro Air Vehicle Conference and Flight Competition (EMAV2007), 17-21 September 2007, Toulouse, France

Nonlinear Attitude and Position Control of a Micro Quadrotor using Sliding Mode and Backstepping Techniques

Patrick Adigbli*

Technische Universität München, 80290 München, Germany and

Christophe Grand† and Jean-Baptiste Mouret‡ and Stéphane Doncieux§

ISIR, Institut des Systèmes Intelligents et Robotique, 75016 Paris, France

The present study addresses the issues concerning the developpment of a reliable assisted remote control for a four-rotor miniature aerial robot (known as quadrotor), guaranteeing the capability of a stable autonomous flight. The following results are proposed: after establishing a dynamical flight model as well as models for the rotors, gears and motors of the quadrotor, different nonlinear control laws are investigated for attitude and position control of the UAV. The stability and performance of feedback, backstepping and sliding mode controllers are compared in simulations. Finally, experiments on a newly implemented quadrotor prototype have been conducted in order to validate the theoretical analysis.

I. Introduction

As their application potential both in the military and industrial sector strongly increases, miniature unmanned aerial vehicles (UAV) constantly gain in interest among the research community. Mostly used for surveillance and inspection roles, building exploration or missions in unaccessible or dangerous environments, the easy handling of the UAV by an operator without hours of training is primordial. In order to develop a reliable assisted remote control or guarantee the capability of a stable autonomous flight, the development of simple and robust control laws stabilizing the UAV becomes more and more important.

This article addresses the design and analysis of nonlinear attitude and position controllers for a four-rotor aerial robot, better known as quadrotor. This aircraft has been chosen for its specific characteristics such as the possibility of vertical take off and landing (VTOL), stationary and quasi-stationary flight and high manoeuverability. Moreover, its simple mechanical structure compared to a helicopter with variable pitch angle rotors and its highly nonlinear, coupled and underactuated dynamics make it an interesting research platform.

The present article proposes the following results: in the second part, models for the propulsion system and the flight dynamic of the UAV are proposed. In the third part, different nonlinear control laws to stabilize the attitude of the quadrocopter are investigated. In the fourth part, a new position controller for autonomous waypoint tracking is designed, using the backstepping approach. Finally, the performance of the investigated controllers are compared in simulations and experiments on a real system. For that purpose, a prototype of the quadrocopter has been implemented.

II. Modelling the electromechanical system

In this section, a complete model of the quadrocopter system is established. First, a model of the propulsion system represented in Fig.1 is proposed, deriving theoretical linear and nonlinear models for the rotor, gear and motor.

*Master student TUM/ECP, Institute of Automatic Control Engineering, patrick.adigbli@centraliens.net

†Prof. assistant, dept SIMA, grand@robot.juiisu.fr

‡PhD student, dept SIMA, Jean-Baptiste.Mouret@lip6.fr

§Prof. assistant, dept SIMA, Stephane.Doncieux@upmc.fr

The reactive torque τ_R caused by the drag of the rotor blade and the thrust f are proportional to the square of the rotational velocity ω of the rotor (see McKerrow et al.[1]):

$$f = k_l\,\omega^2, \qquad \tau_R = k_d\,\omega^2 \tag{1}$$

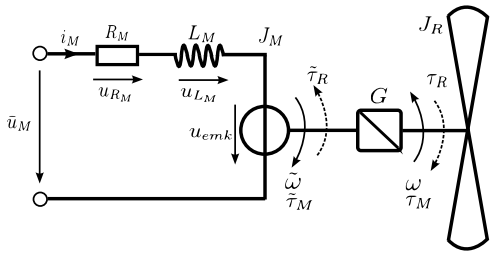

Figure 1. Propulsion system.

The gear is located between the rotor and the couple-generating motor[a], in order to transmit the mechanical power while changing the motor couple τ_M and the rotational velocity ω. Considering the mechanical losses by introducing the efficiency factor η_G, the gear reduction ratio G as well as the total torque of inertia $\tilde{J}_{tot}$ on the motor side can be calculated:

$$G = \frac{\tilde{\omega}}{\omega} = \frac{\tau_M}{\tilde{\tau}_M}\frac{1}{\eta_G} \quad \text{and} \quad \tilde{J}_{tot} = \frac{J_R}{G^2} + J_M \tag{2}$$

The well-known electromechanical model of the dc motor is described by the two following equations, introducing the back-EMF constant k_{emk} and the torsional constant k_M:

$$L_M\,\dot{i}_M = \bar{u}_M - R_M\,i_M - k_{emk}\,\omega \tag{3}$$

$$\tilde{J}_{tot}\,\dot{\tilde{\omega}} = \tilde{\tau}_M - \tilde{\tau}_R = k_M\,i_M - \tilde{\tau}_R \tag{4}$$

With respect to the fact that the motor inductivity L_M can be considered small in comparison to the motor resistance R_M, the system dynamic can be reduced. By taking into account the equations (1) and (2), the simplified nonlinear model for the propulsion system is:

$$\dot{\omega} = \frac{k_M}{R_M\,G\,\tilde{J}_{tot}}\,\bar{u}_M - \frac{k_M\,k_{emk}}{R_M\,G\,\tilde{J}_{tot}}\,\omega - \frac{k_d}{G^2\,\eta_G\,\tilde{J}_{tot}}\,\omega^2 \tag{5}$$

The stationary response curve can be linearized around the operating point $(\omega^*, \bar{u}_M^*)$, finally leading to the simplified and linearized propulsion system model used in this article [b]:

$$\omega = \frac{K_1}{T\,s+1}\,\bar{u}_M + \frac{K_2}{T\,s+1} \tag{6}$$

This model has been verified by an experimental analysis on the propulsion system, using the Least-Square-Fitting method.

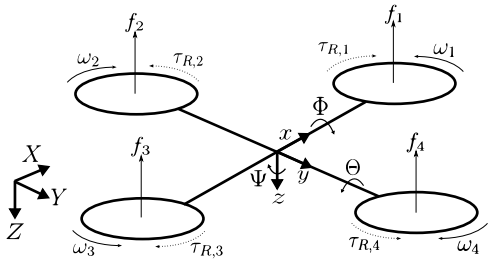

Figure 2. Representation of the quadrotor system, introducing torques, forces and coordinate systems.

After proposing the model of the electromechanical propulsion system, a simplified quasi-stationary flight dynamic model based on the work of Lozano et al.[2] and Bouabdallah and al.[3] will be established. Considering the whole quadrotor system represented in Fig.2, the earth-fixed coordinate system $\boldsymbol{S_W} = [\boldsymbol{X}, \boldsymbol{Y}, \boldsymbol{Z}]^T$ and the body-fixed coordinate system $\boldsymbol{S_{uav}} = [\boldsymbol{x}, \boldsymbol{y}, \boldsymbol{z}]^T$ are introduced. The position $\boldsymbol{\xi} = [x, y, z]^T$ of the UAV is given by the position of the origin of the body-fixed coordinate system relativ to the origin of the earth coordinate system. The orientation of the UAV in space is described by the Tait-Bryan-angles $\boldsymbol{\eta} = [\Phi, \Theta, \Psi]^T$ and the rotation matrix $\boldsymbol{R}$ [c]:

[a] All variables on the *motor side* are marked with a tilde, while all variables on the *rotor side* aren't marked.

[b] With the parameters:

$$K_1 = \frac{\eta_G\,G\,k_M}{2\,k_d\,\omega^*\,R_M + \eta_G\,G\,k_{emk}\,k_M}, \quad K_2 = \frac{k_d\,\omega^{*2}\,R_M}{2\,k_d\,\omega^*\,R_M + \eta_G\,G\,k_{emk}\,k_M}, \quad T = \frac{\eta_G\,G^2\,\tilde{J}_{tot}\,R_M}{2\,k_d\,\omega^*\,R_M + \eta_G\,G\,k_{emk}\,k_M}$$

[c] In this article, the representation of the rotation matrix $\boldsymbol{R}$ is based on the following rotation order: the first rotation with the angle Φ around the x-axis, the second rotation with the angle Θ around the new y-axis and the third rotation with the angle Ψ around the new z-axis.

$$\boldsymbol{R} = \begin{pmatrix} c_\Theta c_\Psi & s_\Phi s_\Theta c_\Psi - c_\Phi s_\Psi & c_\Phi s_\Theta c_\Psi + s_\Phi s_\Psi \\ c_\Theta s_\Psi & s_\Phi s_\Theta s_\Psi + c_\Phi c_\Psi & c_\Phi s_\Theta s_\Psi - s_\Phi c_\Psi \\ -s_\Theta & s_\Phi c_\Theta & c_\Phi c_\Theta \end{pmatrix} \tag{7}$$

The angular rotation velocities $\boldsymbol{\Omega}$ in the body-fixed coordinates can be obtained with respect to the angular rotation velocities $\dot{\boldsymbol{\eta}}$ in the earth-fixed coordinates:

$$\boldsymbol{\Omega} = \begin{pmatrix} 1 & 0 & -s_\Theta \\ 0 & c_\Phi & s_\Phi c_\Theta \\ 0 & -s_\Phi & c_\Phi c_\Theta \end{pmatrix} \dot{\boldsymbol{\eta}} = \boldsymbol{W}(\boldsymbol{\eta})\, \dot{\boldsymbol{\eta}} \tag{8}$$

Now, a full dynamical model of the position and angular acceleration of the quadrocopter is derived, showing that the Euler-Lagrange-formalism, which is also used in the work of Lozano et al.,[2] leads to the same results as the Newton-Euler approach used by Bouabdallah et al.[3] Introducing $\boldsymbol{\rho} = [\boldsymbol{\xi}, \boldsymbol{\eta}]^T$ and applying the Hamilton principle to the Lagrange function $\mathcal{L}(\boldsymbol{\rho}, \dot{\boldsymbol{\rho}}) = \mathcal{T}(\boldsymbol{\rho}, \dot{\boldsymbol{\rho}}) - \mathcal{V}(\boldsymbol{\rho})$ composed of the kinetic and potential energies $\mathcal{T}$ and $\mathcal{V}$ of the global mechanical system leads to the Euler-Lagrange-equations:

$$\frac{d}{dt}\left(\frac{\partial \mathcal{L}}{\partial \dot{\boldsymbol{\rho}}_i}\right) - \frac{\partial \mathcal{L}}{\partial \boldsymbol{\rho}_i} = Q_i \qquad \text{with} \quad i = 1 \ldots 6 \tag{9}$$

First, all components of the Lagrange function $\mathcal{L}$ and the generalized potential-free force vector $\boldsymbol{Q}$ have to be identified. Both can be divided in a translational and a rotational part:

$$\mathcal{L}_{trans} = \mathcal{T}_{trans} - \mathcal{V} = \frac{1}{2}\, m_{uav}\, \dot{\boldsymbol{\xi}}^T\, \dot{\boldsymbol{\xi}} + m_{uav}\, g\, z \qquad \boldsymbol{Q}_{trans} = \boldsymbol{R} \begin{pmatrix} 0 \\ 0 \\ -F \end{pmatrix}$$

$$\mathcal{L}_{rot} = \mathcal{T}_{rot} = \frac{1}{2}\, \boldsymbol{\Omega}^T\, \boldsymbol{I}\, \boldsymbol{\Omega} = \frac{1}{2}\, \dot{\boldsymbol{\eta}}^T\, \boldsymbol{J}\, \dot{\boldsymbol{\eta}} \qquad \boldsymbol{Q}_{rot} = \boldsymbol{\tau} + \boldsymbol{\tau}_{gyro} = \begin{pmatrix} 0 & l\,k_l & 0 & -l\,k_l \\ l\,k_l & 0 & -l\,k_l & 0 \\ k_d & -k_d & k_d & -k_d \end{pmatrix} \boldsymbol{\omega}^2 + \sum_{i=1}^{4} J_R\, (\boldsymbol{\Omega} \times \boldsymbol{e}_z)\, (-1)^{i+1}\, \omega_i$$

Now, the Euler-Lagrange-equations for position and orientation can be deduced independently:

$$\begin{aligned} \boldsymbol{Q}_{trans} &= \tfrac{d}{dt}\left(\tfrac{\partial \mathcal{L}_{trans}}{\partial \dot{\boldsymbol{\xi}}}\right) - \tfrac{\partial \mathcal{L}_{trans}}{\partial \boldsymbol{\xi}} \\ \boldsymbol{Q}_{rot} &= \tfrac{d}{dt}\left(\tfrac{\partial \mathcal{L}_{rot}}{\partial \dot{\boldsymbol{\eta}}}\right) - \tfrac{\partial \mathcal{L}_{rot}}{\partial \boldsymbol{\eta}} \end{aligned} \quad \Leftrightarrow \quad \begin{aligned} \ddot{\boldsymbol{\xi}} &= \tfrac{\boldsymbol{Q}_{trans}}{m_{uav}} + \begin{pmatrix} 0 \\ 0 \\ g \end{pmatrix} \\ \ddot{\boldsymbol{\eta}} &= \boldsymbol{J}^{-1} \left(\boldsymbol{Q}_{rot} + \tfrac{1}{2}\, \tfrac{\partial}{\partial \boldsymbol{\eta}} \left(\dot{\boldsymbol{\eta}}^T\, \boldsymbol{J}\, \dot{\boldsymbol{\eta}} \right) - \boldsymbol{J}\, \dot{\boldsymbol{\eta}} \right) \end{aligned} \tag{10}$$

After considering the hypothesis of small angles and small angular velocities, the full dynamical model (10) can be simplified, resulting in a nonlinear coupled model containing terms for the coriolis forces and gyroscopic torques:

$$\begin{aligned} \ddot{x} &= -\tfrac{F}{m_{uav}}\, (c_\Phi\, c_\Psi\, s_\Theta + s_\Phi\, s_\Psi) \\ \ddot{y} &= -\tfrac{F}{m_{uav}}\, (c_\Phi\, s_\Psi\, s_\Theta - s_\Phi\, c_\Psi) \\ \ddot{z} &= -\tfrac{F}{m_{uav}}\, (c_\Phi\, c_\Theta) + g \end{aligned} \qquad \begin{aligned} \ddot{\Phi} &= \tfrac{\tau_\Phi}{I_x} - \tfrac{J_R\, \Pi}{I_x}\, \dot{\Theta} + \dot{\Theta}\, \dot{\Psi} \left(\tfrac{I_y - I_z}{I_x}\right) \\ \ddot{\Theta} &= \tfrac{\tau_\Theta}{I_y} + \tfrac{J_R\, \Pi}{I_y}\, \dot{\Phi} + \dot{\Phi}\, \dot{\Psi} \left(\tfrac{I_z - I_x}{I_y}\right) \\ \ddot{\Psi} &= \tfrac{\tau_\Psi}{I_z} + \dot{\Phi}\, \dot{\Theta} \left(\tfrac{I_x - I_y}{I_z}\right) \end{aligned} \tag{11}$$

III. Attitude stabilization

In a next step, different nonlinear control laws for the control torque vector $\boldsymbol{\tau}^{ctrl} = [\boldsymbol{\tau}_\Phi^{ctrl}, \boldsymbol{\tau}_\Theta^{ctrl}, \boldsymbol{\tau}_\Psi^{ctrl}]^T$ are investigated in order to stabilize the highly nonlinear, underactuated system, even in presence of perturbations. The control architecture represented in Fig.3 remains the same for the different control laws.

First, a quaternion-based feedback controller presented by Tayebi et al.[4] has been chosen for its model parameter independent, simple implementation:

$$\boldsymbol{\tau}^{ctrl} = -\mu_q \left(\boldsymbol{q} - \boldsymbol{q}^d\right) - \boldsymbol{\mu}\,\boldsymbol{\Omega} \tag{12}$$

with the reduced quaternion vector $\boldsymbol{q} = [q_1, q_2, q_3]^T$, the positive parameter μ_q and the positive definite 3x3 diagonal matrix $\boldsymbol{\mu}$. It is shown in[4] that the control law is globally asymptotically stable.

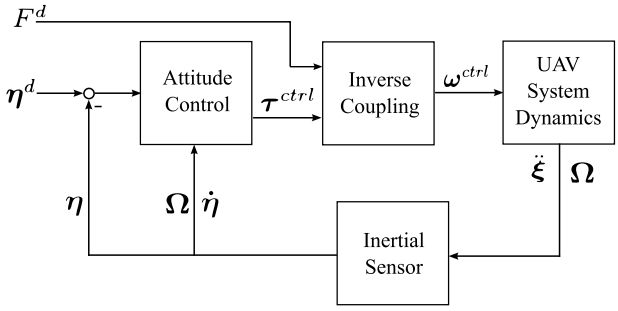

Figure 3. Attitude control architecture.

The second controller has been derived using the backstepping approach, especially adapted to the present system, where the states of the rotational subsystem can be considered as inputs for the translational subsystem. First, the dynamical model from (11) is rewritten as:

$$\begin{aligned} x_1 &= \Phi & x_3 &= \Theta & x_5 &= \Psi \\ x_2 &= \dot{x_1} = \dot{\Phi} & x_4 &= \dot{x_3} = \dot{\Theta} & x_6 &= \dot{x_5} = \dot{\Psi} \\ \dot{x_2} &= \ddot{\Phi} & \dot{x_4} &= \ddot{\Theta} & \dot{x_6} &= \ddot{\Psi} \end{aligned}$$

Next, the $\boldsymbol{x}$-coordinates are transformed into new $\boldsymbol{z}$-coordinates by means of a diffeomorphism. This is illustrated using the x_1, x_2-coordinates:

$$\begin{aligned} z_1 &= x_1 - x_1^d, \quad z_2 = x_2 - \dot{x}_1^d - \alpha_1(z_1), \\ \dot{z_1} &= \dot{x}_1 - \dot{x}_1^d = z_2 + \alpha_1(z_1) \end{aligned}$$

By introducing the partial lyapunov functions $V_1 = \frac{1}{2} z_1^2$ and $V_2 = \frac{1}{2}\left(z_1^2 + z_2^2\right)$, it is possible to determine the function $\alpha_1(z_1)$, two parameters $a_1, a_2 > 0$ and the control law for τ_Φ such that the derivate $\dot{V}_2 \equiv -\sum_{i=1}^{2} a_i z_i^2 < 0$. Therefore, referring to the lyapunov stability theorem, the global asymptotical stability of the equilibrium point $\boldsymbol{z}^* = \boldsymbol{0}$ is guaranteed and Φ tends to Φ^d. Applying this procedure to all $\boldsymbol{x}$-coordinates and assuming that $\ddot{\boldsymbol{\eta}}^d = \dot{\boldsymbol{\eta}}^d = \boldsymbol{0}$ and $\dot{\boldsymbol{\eta}} \simeq \boldsymbol{\Omega}$, one obtains the following backstepping control law:

$$\begin{aligned} \boldsymbol{\tau}^{ctrl} = &- \boldsymbol{I} \begin{pmatrix} a_1\, a_2{-}1 & 0 & 0 \\ 0 & a_3\, a_4{-}1 & 0 \\ 0 & 0 & a_5\, a_6{-}1 \end{pmatrix} (\boldsymbol{\eta} - \boldsymbol{\eta}^d) \\ &- \boldsymbol{I} \begin{pmatrix} a_1{+}a_2 & 0 & 0 \\ 0 & a_3{+}a_4 & 0 \\ 0 & 0 & a_5{+}a_6 \end{pmatrix} \boldsymbol{\Omega} \end{aligned} \tag{13}$$

In accordance with the previous work of Wendel et al.,[5] it will be shown in section V that in realistic scenarios the performance of the derived backstepping controller is superior to the feedback controller.

Eventually, a new sliding mode attitude controller is proposed in this article. Based on the works of Utkin, Kondak et al. and Brandstätter et al.,[6–8] this approach is more robust against parameter uncertainties and perturbations and can easily be implemented. In comparision to the work of Bouabdallah et al.,[3] the proposed sliding mode controller is much simpler, shows good performances in realistic simulations of the complet UAV system and its stability is formally proven.
Introducing the extended state vector $\boldsymbol{x} = [\boldsymbol{\eta}, \dot{\boldsymbol{\eta}}]^T$ and the input vector $\boldsymbol{u} = \boldsymbol{\tau} = [\tau_\Phi, \tau_\Theta, \tau_\Psi]^T$, the system behaviour can be described as:

$$\dot{\boldsymbol{x}} = \boldsymbol{f}(\boldsymbol{x}) + \boldsymbol{B}(\boldsymbol{x})\boldsymbol{u} \quad \Leftrightarrow \quad \begin{aligned} \boldsymbol{v} &= \dot{\boldsymbol{\eta}} \\ \dot{\boldsymbol{v}} &= \ddot{\boldsymbol{\eta}} \end{aligned} \tag{14}$$

The control error and its derivative are given by $\boldsymbol{e} = \boldsymbol{\eta} - \boldsymbol{\eta}^d, \dot{\boldsymbol{e}} = \dot{\boldsymbol{\eta}} - \dot{\boldsymbol{\eta}}^d = \dot{\boldsymbol{\eta}}$ and the switching or sliding manifolds $\boldsymbol{S}$ are characterized by $\boldsymbol{S} = \left\{\boldsymbol{x} \in \mathbf{R}^3 \,|\, \boldsymbol{s}(\boldsymbol{x}) = \boldsymbol{0}\right\}$ with $\boldsymbol{s}(\boldsymbol{x}) = \boldsymbol{C}_1\,\boldsymbol{e} + \boldsymbol{C}_2\,\dot{\boldsymbol{e}}$, where $\boldsymbol{C}_1, \boldsymbol{C}_2$ are two diagonal matrices. To achieve motion along these sliding manifolds, a discountinuous control law is used:

$$\boldsymbol{u}^{ctrl}(\boldsymbol{x}) = -K\,\mathrm{sign}\left(\boldsymbol{s}(\boldsymbol{x})\right) = \begin{cases} \boldsymbol{u}_+(\boldsymbol{x}), & \boldsymbol{s}(\boldsymbol{x}) > 0 \\ \boldsymbol{u}_-(\boldsymbol{x}), & \boldsymbol{s}(\boldsymbol{x}) < 0 \end{cases} \tag{15}$$

In order to formally prove the stability of this sliding mode controller, the following two assumptions have to be verified:

1. The system has to reach the sliding manifolds S_i after a finite time, independently from the systems initial state $\boldsymbol{x_0}$.
2. The motion along the sliding manifolds S_i must have a stable behaviour.

In order to verify the second assumption, Utkins *equivalent control method* will be used:[6] therefore, a continuous equivalent control variable $\boldsymbol{u_{eq}}$ must exist and verify the condition:

$$\min(\boldsymbol{u}) \leq \boldsymbol{u_{eq}} \leq \max(\boldsymbol{u}) \tag{16}$$

In the sliding mode, $\boldsymbol{u_{eq}}$ replaces $\boldsymbol{u}$ and with (14), we have $\dot{\boldsymbol{s}}(\boldsymbol{x}) = \boldsymbol{0}$ and $\dot{\boldsymbol{s}}(\boldsymbol{x}) = \frac{\partial \boldsymbol{s}}{\partial \boldsymbol{x}}\,\dot{\boldsymbol{x}} = \frac{\partial \boldsymbol{s}}{\partial \boldsymbol{x}}\,(\boldsymbol{f}(\boldsymbol{x}) + \boldsymbol{B}\,\boldsymbol{u_{eq}})$. Consequently, the equivalent control is given by:

$$\boldsymbol{u_{eq}} = -\left(\frac{\partial \boldsymbol{s}}{\partial \boldsymbol{x}}\,\boldsymbol{B}\right)^{-1} \frac{\partial \boldsymbol{s}}{\partial \boldsymbol{x}}\,\boldsymbol{f}(\boldsymbol{x}) \quad \text{with} \quad \frac{\partial \boldsymbol{s}}{\partial \boldsymbol{x}}\boldsymbol{B} = \begin{pmatrix} c_4/I_x & 0 & 0 \\ 0 & c_5/I_y & 0 \\ 0 & 0 & c_6/I_z \end{pmatrix} \tag{17}$$

The existence of $\boldsymbol{u_{eq}}$ is guaranteed, because the inverse of $\frac{\partial \boldsymbol{s}}{\partial \boldsymbol{x}}\boldsymbol{B}$ exists and the components of the term $\frac{\partial \boldsymbol{s}}{\partial \boldsymbol{x}}\,\boldsymbol{f}(\boldsymbol{x})$ could become zero only in single isolated points of the state space. Thus, the second assumption is partially verified, only (16) has to be satisfied. To guarantee this, we consider assumption 1, which is equivalent to finding the so called *domain of sliding mode* and can be reduced to a stability problem with the state vector $\boldsymbol{s}$ and the lyapunov function $V(\boldsymbol{s}) = \operatorname{sign}(\boldsymbol{s})^T\,\boldsymbol{s}$. Considering (14), (17) and (15), the derivative of V is:

$$\dot{V}(\boldsymbol{s}) = -K \operatorname{sign}(\boldsymbol{s})^T \frac{\partial \boldsymbol{s}}{\partial \boldsymbol{x}}\,\boldsymbol{B} \operatorname{sign}(\boldsymbol{s}) - \operatorname{sign}(\boldsymbol{s})^T \frac{\partial \boldsymbol{s}}{\partial \boldsymbol{x}}\,\boldsymbol{B}\,\boldsymbol{u_{eq}}$$

Because $\frac{\partial \boldsymbol{s}}{\partial \boldsymbol{x}}\,\boldsymbol{B}$ is positive definite, the first term of $\dot{V}$ is confined to $c_{min}\,\|\operatorname{sign}(\boldsymbol{s})\|^2 \leq \operatorname{sign}(\boldsymbol{s})^T\,\frac{\partial \boldsymbol{s}}{\partial \boldsymbol{x}}\,\boldsymbol{B} \operatorname{sign}(\boldsymbol{s}) \leq c_{max}\,\|\operatorname{sign}(\boldsymbol{s})\|^2$ with $c_{min} = \min\left\{\frac{c_4}{I_x}, \frac{c_5}{I_y}, \frac{c_6}{I_z}\right\}$ and $c_{max} = \max\left\{\frac{c_4}{I_x}, \frac{c_5}{I_y}, \frac{c_6}{I_z}\right\}$ and we have:

$$\dot{V}(\boldsymbol{s}) \leq -\mathrm{K}\,c_{min}\,\|\operatorname{sign}(\boldsymbol{s})\|^2 + \|\operatorname{sign}(\boldsymbol{s})^T\|\,\|\frac{\partial \boldsymbol{s}}{\partial \boldsymbol{x}}\,\boldsymbol{B}\|\,\|\boldsymbol{u_{eq}}\|$$

Outside of the sliding manifolds $\boldsymbol{S}_i$, we have $\|\operatorname{sign}(\boldsymbol{s})\| \geq 1$, because at least one component $s_i \neq 0$. Therefore, the derivative of the lyapunov function is negative, when we have:

$$K > \frac{\|\frac{\partial \boldsymbol{s}}{\partial \boldsymbol{x}}\,\boldsymbol{B}\|\,\|\boldsymbol{u_{eq}}\|}{c_{min}} \tag{18}$$

By choosing K according to (18), the domain of sliding mode corresponds to the whole state space, verifying assumption 1. Furthermore, we will now show that (16) $\Leftrightarrow -K \leq \boldsymbol{u_{eq}} \leq +K \quad \Rightarrow \|\boldsymbol{u_{eq}}\| \leq K$ is satisfied by this choice of K. Considering the Frobeniusnorm $\|\frac{\partial \boldsymbol{s}}{\partial \boldsymbol{x}}\,\boldsymbol{B}\|_F^2 = \left(\frac{c_4}{I_x}\right)^2 + \left(\frac{c_5}{I_y}\right)^2 + \left(\frac{c_6}{I_z}\right)^2$, the stability of the sliding mode controller is formally proven, because we have:

$$\|\boldsymbol{u_{eq}}\| < \mathrm{K}\,\frac{c_{min}}{\|\frac{\partial \boldsymbol{s}}{\partial \boldsymbol{x}}\,\boldsymbol{B}\|_F} \leq \mathrm{K} \tag{19}$$

IV. Position control

Another main contribution of the present article is the design of a position controller based on the backstepping approach. The superposition of the position controller over the attitude controller in a cascade architecture (shown in Fig.4) enables the robot to perform autonomous waypoint tracking: the operator or path planner provides the desired values x^d, y^d, z^d and Ψ^d and the position controller calculates the corresponding control values $\Phi^{ctrl}, \Theta^{ctrl}$ and F^{ctrl}, which represent the set values of the underlying attitude

controller. To derive the backstepping position control law, a diffeomorphism transforms the position vector $\boldsymbol{\xi} = [x, y, z]^T$ into $\boldsymbol{z}$-coordinates. This operation will be illustrated using the x-coordinate:

$$z_1 = x - x^d, \quad z_2 = \dot{x} - \dot{x}^d - \beta_1(z_1),$$
$$\dot{z_1} = \dot{x} - \dot{x}^d = z_2 + \beta_1(z_1)$$

By introducing the partial lyapunov functions $V_1 = \frac{1}{2}z_1^2$ and $V_2 = \frac{1}{2}\left(z_1^2 + z_2^2\right)$, it is possible to determine the function $\beta_1(z_1)$ and two parameters $b_1, b_2 > 0$ such that the derivate $\dot{V_2} \equiv -\sum_{i=1}^{2} b_i z_i^2 < 0$:

$$\beta_1 = -b_1 z_1$$

$$\dot{V_2} = z_1\,\dot{z}_1 + (\dot{z}_1 - \beta(z_1))(\ddot{z}_1 - \dot{\beta}_1) \equiv -\sum_{i=1}^{2} b_i z_i^2 \;\Leftrightarrow\; z_1 + \ddot{z}_1 + b_1\,\dot{z}_1 + b_2\,z_2 = 0$$

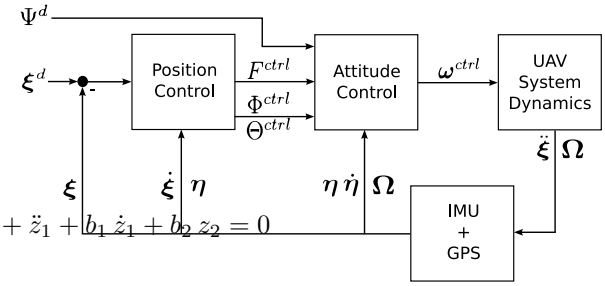

Figure 4. Cascade control architecture.

After applying the same procedure to the y and z-coordinates and retransforming from $\boldsymbol{z}$ to $\boldsymbol{\xi}$-coordinates, we obtain:

$$\begin{array}{lll} -\frac{F}{m_{uav}}\left(c_\Phi\, c_{\Psi^d}\, s_\Theta + s_\Phi\, s_{\Psi^d}\right) + r_1 = 0 & & r_1 = (1 + b_1\, b_2)\,(x - x^d) + (b_1 + b_2)\,\dot{x} \\ -\frac{F}{m_{uav}}\left(c_\Phi\, s_\Theta\, c_{\Psi^d} + s_\Phi\, s_{\Psi^d}\right) + r_2 = 0 & \text{with} & r_2 = (1 + b_3\, b_4)\,(y - y^d) + (b_3 + b_4)\,\dot{y} \\ -\frac{F}{m_{uav}}\left(c_\Phi\, c_\Theta\right) + g + r_3 = 0 & & r_3 = (1 + b_5\, b_6)\,(z - z^d) + (b_5 + b_6)\,\dot{z} \end{array} \tag{20}$$

Considering that x^d, y^d, z^d and Ψ^d are known and $\boldsymbol{\eta}, \boldsymbol{\xi}, \dot{\boldsymbol{\xi}}$ can be measured, the equations (20) can be solved in order to determine the control variables $\Phi^{ctrl}, \Theta^{ctrl}$ and F^{ctrl}, [d] obtaining the following backstepping position controller:

$$\begin{aligned} F^{ctrl} &= \frac{m_{uav}}{c_\Phi\, c_\Theta}\,(r_3 + g) \\ \Phi^{ctrl} &= \arcsin\left(\frac{m_{uav}}{F^{ctrl}}\,(r_1\, s_{\Psi^d} - r_2\, c_{\Psi^d})\right) \\ \Theta^{ctrl} &= \arcsin\left(\frac{m_{uav}}{F^{ctrl}\, c_{\Phi^{ctrl}}}\,(r_1\, c_{\Psi^d} + r_2\, s_{\Psi^d})\right) \end{aligned} \tag{21}$$

V. Simulation and experimental results

In order to evaluate and compare the investigated control laws, various simulations have been performed on the complete closed loop system. The models for the propulsion group (6) and the flight dynamics (11) have been implemented in *scilab/scicos* and the following disturbances have been added: the motor dynamics are delayed and bounded, the measured angles are overlaid with an additive gaussian noise (mean value $\mu = 0°$, standard deviation $\sigma = 2°$), the digitally implemented controllers work at a frequency of 50 Hz and the control output is bounded.

In the first simulation, all control laws have to stabilize the attitude of the UAV, bringing it from an initially inclined to a horizontal configuration ($\boldsymbol{\eta}^d = \mathbf{0}$) within approximately 1 sec: as seen in Fig.5, it appears that for this task the performance of the control laws is comparable. Furthermore, a scenario has been simulated, where each controller has to track a given setpoint, bringing the attitude from the UAV from an initial configuration $\boldsymbol{\eta} = \mathbf{0}$ to the desired configuration $\boldsymbol{\eta}^d = [30°, 20°, -45°]^T$ within approximately 2 seconds: Fig.6 shows that in our simulations the necessary high gains for this short convergence time make the behaviour of the feedback controller unstable, whereas the backstepping and sliding mode controller behave well.

[d] To rule out trigonometric singularities, the argument of arcsin() has to be limited to $[-1; 1]$ and the angles Φ and Θ have to be limited to $]-\frac{\pi}{2}; +\frac{\pi}{2}[$.

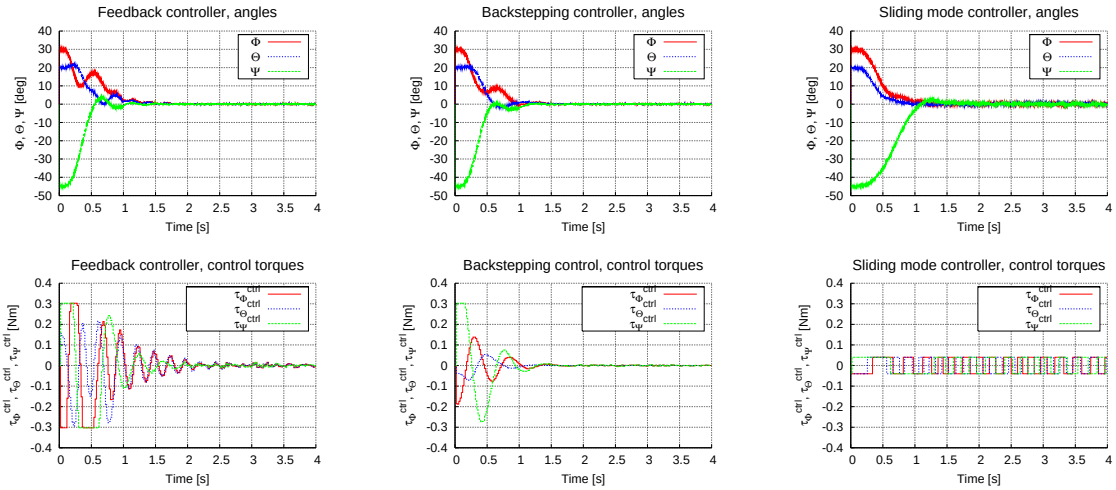

Figure 5. Simulation results of the attitude stabilisation, $\boldsymbol{\eta}^d = [0°, 0°, 0°]^T$. Top row: angles with feedback control (left), backstepping control (middle), sliding mode control (right). Bottom row: control torques with feedback control (left), backstepping control (middle), sliding mode control (right). Controller parameters: $\mu_x = \mu_y = \mu_z = 0.4, \mu_q = 10, a_1 = a_2 = a_4 = a_6 = 7, a_3 = 2, a_5 = 5, K = 0.04, c_1 = c_3 = c_5 = 1, c_2 = 0.3, c_4 = 0.5, c_6 = 0.4$

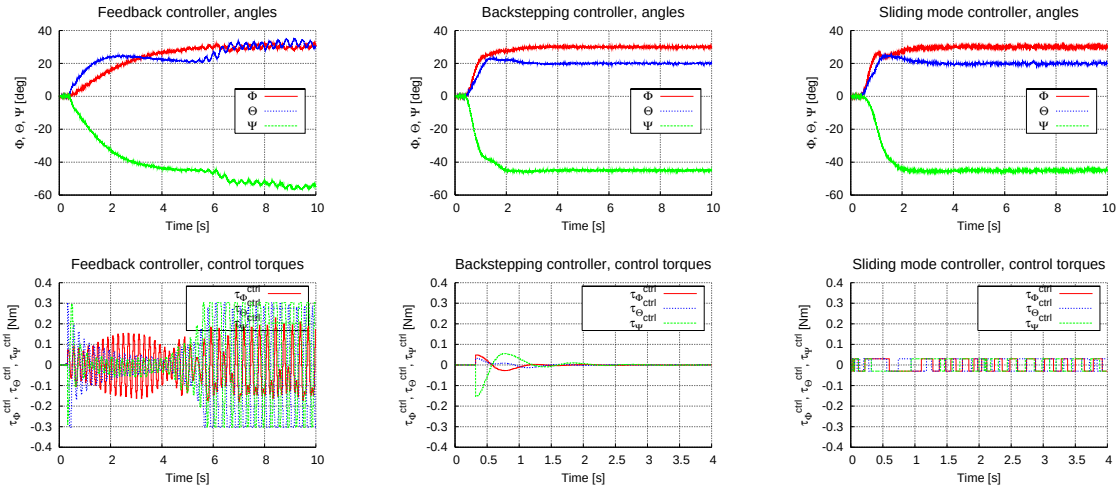

Figure 6. Simulation results of the setpoint tracking, $\boldsymbol{\eta}^d = [30°, 20°, -45°]^T$. Top row: angles with feedback control (left), backstepping control (middle), sliding mode control (right). Bottom row: control torques with feedback control (left), backstepping control (middle), sliding mode controller (right). Controller parameters: $\mu_x = \mu_y = \mu_z = 0.7, \mu_q = 5, a_1 = a_3 = a_5 = 4, a_2 = a_4 = a_6 = 3, K = 0.03, c_1 = c_3 = c_5 = 1, b_2 = 0.4, b_4 = b_6 = 0.5$

For the validation of the position controller, various scenarios have been simulated, showing promissing results for an implementation on the real system. For example, the UAV has to follow a helix formed path while rotating around his own z-axis: the simulation result is represented in Fig.7, showing the stable tracking behaviour of the complete closed loop system.

Moreover, a low cost autonomous miniature drone (represented in Fig.8) has been designed and implemented, using exclusively off-the-shelf components and open source software: employing a highly integrated embedded inertial measurement unit discussed in the work of Jang et al.[9] and the power of a real time onboard CPU, the backstepping control law has been implemented on the real system suspended on a tripod. Fig.9 shows some first test results obtained with the prototype, which is stabilized around $\boldsymbol{\eta} = \mathbf{0}$. Improvements have still to be made on the hardware to enhance the controller dynamics, particularly with regard to the closed-loop speed control of the motors.

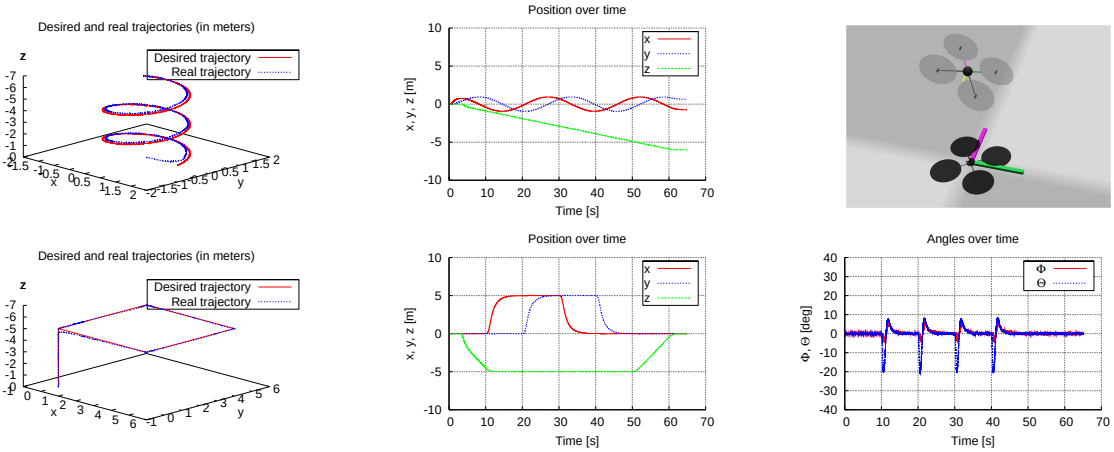

Figure 7. Simulation results of the position controller. Top row: the UAV tracks well the desired path in form of a helix (left), it's actual position ξ is plotted (middle) and a 3D-animation (right) visualizes the simulation results. Bottom row: the UAV tracks well the desired quadratic path (left), it's actual position ξ is plotted (middle) and the angular values Φ, Θ are plotted (right). Attitude controller parameters: $a_1 = a_2 = a_3 = a_4 = a_5 = a_6 = 7, b_1 = b_2 = 5, b_3 = b_5 = 1, b_4 = b_6 = 2$

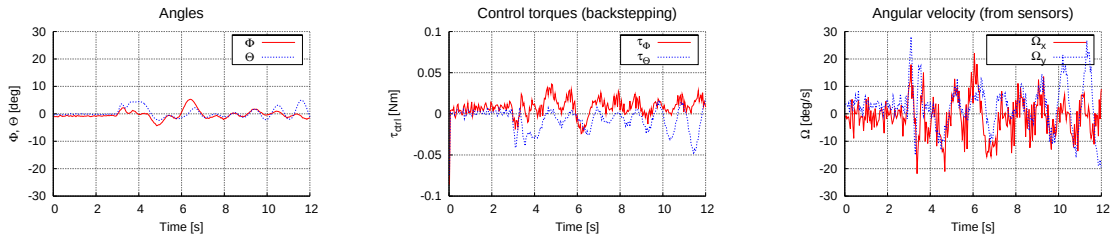

Figure 9. First test results of the backstepping attitude controller.

VI. Conclusion

In this article, a complete and a simplified model for a four-rotor flying robot have been proposed. Moreover, three different control approaches have been investigated and discussed: a feedback control law, a backstepping control law and a newly established sliding mode control law. The performances have been analysed using various simulation results, showing the robust behaviour of the backstepping and sliding mode controllers regarding the stabilization and the setpoint tracking of the complete UAV model, whereas the feedback controller shows poor performance regarding the setpoint tracking. Furthermore, a new position controller has been proposed, permitting an autonomous waypoint tracking and showing promissing simulation results. Finally, a low cost prototype has been implemented, showing promissing first test results.

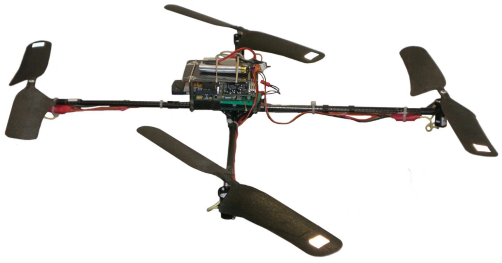

Figure 8. Quadrocopter prototype with an highly integrated Inertial Measurment Unit and a ARM-based CPU running a linux OS.

References

[1]McKerrow, P., "Modelling the Draganflyer four-rotor helicopter," *IEEE International Conference on Robotics and Automation, 2004*, 2004, pp. 3596– 3601.

[2]Escareno, J., Salazar-Cruz, S., and Lozano, R., "Embedded control of a four-rotor UAV," *Proceedings of the 2006 American Control Conference Minneapolis, 2006*, 2005.

[3]Bouabdallah, S. and Siegwart, R., "Backstepping and Sliding-mode Techniques Applied to an Indoor Micro Quadrotor," *IEEE International Conference on Robotics and Automation, 2005*, 2005, pp. 2247– 2252.

[4]Tayebi, A. and McGilvray, S., "Attitude Stabilization of a VTOL Quadrotor Aircraft," *IEEE Transactions on control systems technology, 2006*, Vol. 14, 2006, pp. 562– 571.

[5]Wendel, J. and Bruskowski, L., "Comparison of Different Control Laws for the Stabilization of a VTOL UAV," *European Micro Air Vehicle Conference and Flight Competition 2006 25 - 26.07.2006, Braunschweig*, 2006.

[6]Utkin, V. I., "Variable structure systems with sliding modes," *IEEE Transactions on Automatic Control*, Vol. AC-22, 1977, pp. 212–222.

[7]Kondak, K., Hommel, G., Stanczyk, B., and Buss, M., "Robust Motion Control for Robotic Systems Using Sliding Mode," *Proceedings of the IEEE/RSJ International Conference on Intelligent Robots and Systems, 2005*, 2005, pp. 2375 – 2380.

[8]Brandtstadter, H. and Buss, M., "Control of Electromechanical Systems using Sliding Mode Techniques," *44th IEEE Conference on Decision and Control, 2005 and 2005 European Control Conference*, 2005, pp. 1947 – 1952.

[9]Jang, J. and Liccardo, D., "Automation of small UAVs using a low cost MEMS sensor and embedded computing platform," *25th Digital Avionics Systems Conference, 2006*, 2006.